Chinese Chemical Letters 34 (2023) 107571

Contents lists available at ScienceDirect

Chinese Chemical Letters

journal homepage: www.elsevier.com/locate/cclet

Activating surface atoms of high entropy oxides for enhancing oxygen evolution reaction

Mengyu Li[a], Minglei Song[a], Wenting Ni[a], Zhaohui Xiao[a], Yingying Li[a], Jianfeng Jia[b], Shuangyin Wang[a], Yanyong Wang[a,*]

[a] State Key Laboratory of Chem/Bio-sensing and Chemometrics, College of Chemistry and Chemical Engineering, Hunan University, Changsha 410082, China
[b] Key Laboratory of Magnetic Molecules and Magnetic Information Materials (Ministry of Education), School of Chemistry and Material Science, Shanxi Normal University, Taiyuan 030031, China

ARTICLE INFO

Article history:
Received 3 March 2022
Revised 15 May 2022
Accepted 26 May 2022
Available online 29 May 2022

Keywords:
High entropy oxides
Oxygen evolution reaction
Oxygen vacancies
Low-crystallinity
Leaching

ABSTRACT

High entropy oxides (HEOs) have attracted extensive attention of researchers due to their remarkable properties. The electrocatalytic activity of electrocatalysts is closely related to the reactivity of their surface atoms which usually shows a positive correlation. Excellenet stability of HEOs leads to their surface atoms with relative poor reactivity, limiting the applications for electrocatalysis. Therefore, it is significant to activate surface atoms of HEOs. Constructing amorphous structure, introducing oxygen defects and leaching are very effective strategies to improve the reactivity of surface atoms. Herein, to remove chemical inert, low-crystallinity (Fe, Co, Ni, Mn, Zn)$_3$O$_4$ (HEO-Origin) nanosheets with abundant oxygen vacancies was synthesized, showing an excellent catalytic activity with an overpotential of 265 mV at 10 mA/cm^2, which outperforms as-synthesized HEO-500°C-air (335 mV). The excellent catalytic performance of HEO-Origin can be attributed to high activity surface atoms, the introduction of oxygen defects efficiently altered electron distribution on the surface of HEO-Origin. Apart from, HEO-Origin also exhibits an outstanding electrochemical stability for oxygen evolution reaction (OER).

2015, a new type of oxide material emerged which is known as high entropy oxides (HEOs), possessing unique physical and chemical properties [1–3]. The concept of HEOs is derived from high entropy alloys (HEAs), referring oxides contain five or more cations with an equal or near-equal molar fraction leads to the formation of single-phase crystal structure [4–7]. When all the elements have the same molar fraction, mixing entropy reaches the maximum [8]. According to $G = H - TS$, Gibbs free energy reaches the minimum, indicating the phase of HEOs is the most thermodynamically stable and HEOs have excellent stability [9]. In HEOs, randomly and uniformly distributed of cations and there is no difference between solute and solvent. Due to HEOs possess unique properties, which have various potential applications. For example, $(Co_{0.2}Ni_{0.2}Cu_{0.2}Zn_{0.2}Mg_{0.2})O$ supported Pt was applied to CO oxidation [10], operating at 135 °C for 40 h without the loss of activity due to entropy-stabilization behavior. Moreover, transition metal-based HEO (TM-HEO) of $(MgCoNiCuZn)_{1-x}Li_xO$ possesses high Li-ion conductivity [11], rock $(Co_{0.2}Ni_{0.2}Cu_{0.2}Zn_{0.2}Mg_{0.2})O$ was applied to reversible energy storage [5], providing a possibility to tailor electrochemical performance by changing element composition or element molar fraction. As a result of excellent stability and high coordination saturation, HEOs are difficult to apply to electrocatalysis. It is significant to activate surface atoms of HEOs to promote their application in the field of electrocatalysis.

De-alloying is a promising strategy to activate surface atoms and decrease reaction overpotential [12]. Duan *et al.* through electrochemical de-alloying strategy converted PtNi alloy into jagged platinum nanowires (J-Pt NMs) with 13.6 A/mg$_{Pt}$ for oxygen reduction reaction (ORR) [13]. Ultrahigh mass activity of J-PtNWs can be attributed to low coordination number of surface atoms, decreasing the binding energy of reaction intermediate and the activation energy of ORR rate determining step. Besides, constructing amorphous structure is another efficient strategy to activate surface atoms. Amorphous oxides usually exhibit greater electrocatalytic properties than their crystalline forms [14–16]. Amorphous NiFeMo oxide underwent a rapid surface self-reconstruction process [17], generating favorable electronic and geometric structure and creating active NiFe oxy(hydroxide) layer on the surface of oxide. More importantly, creating defects has been proven that it is an effective way to improve intrinsic activity of active sites. Oxygen vacancy is

* Corresponding author.
E-mail address: yanyongwang@hnu.edu.cn (Y. Wang).

https://doi.org/10.1016/j.cclet.2022.05.085
1001-8417/

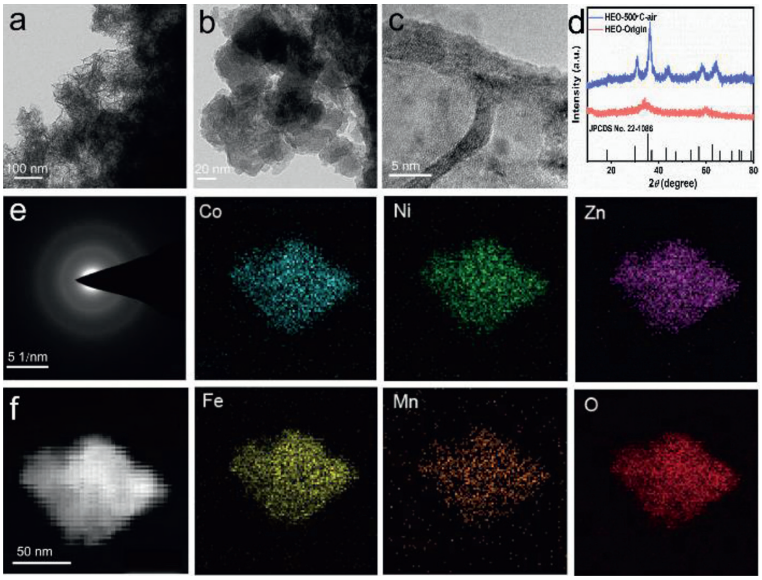

Fig. 1. (a, b) TEM images and (c) HRTEM of HEO-Origin. (d) XRD patterns of HEO-Origin and HEO-500°C-air. (e) SAED pattern and (f) EDS element mappings of HEO-Origin.

one of the most common defect types in transition metal oxides, being able to modulate their electronic structure, band gap, conductivity, and catalytic performance [18–20]. Oxygen vacancies can lower the Gibbs free energy associated with *OOH adsorption, enabling an easier release of oxygen [17]. It is well known that oxygen vacancies can greatly improve OER properties via regulating electronic property, changing the bonding strength of reactants or reaction intermediates, and reducing kinetics barrier [17,21].

Herein, we synthesized a low-crystallinity HEO with abundant oxygen vacancies *via* $NaBH_4$ reduction strategy. Low-crystallinity $(Fe, Co, Ni, Zn, Mn)_3O_4$ (HEO-Origin) nanosheet provides abundant reactive sites and accelerates electron transfer. Abundant oxygen vacancies in HEO-Origin promote the activation of surface atoms, tunes electronic structure, and ultimately enhance intrinsic activity of active sites. As expected, as-synthesized HEO-Origin as OER electrocatalyst showed an excellent electrocatalytic properties and stability.

HEO-Origin was synthesized via a facile $NaBH_4$ reduction strategy. HEO-500°C-air was obtained by calcining HEO-Origin at 500 °C under air atmosphere. HEO-Origin displays curly nanosheets (Fig. S1a in Supporting information). With the increase of calcination temperature, the size of catalysts increased dramatically (Figs. S1b-f in Supporting information). As the temperature continues to rise to 900 °C, the size of nanosheets ranges from hundreds of nanometres to micrometres. Transmission electron microscopy (TEM) also indicates HEO-Origin showed nanosheet feature in Figs. 1a and b. The thickness of HEO-Origin was about 40 nm and the width was 200 nm, which was confirmed by Atomic Force Microscope (AFM) in Fig. S2 (Supporting information). After thermal annealing at 500 °C under air atmosphere, Brunauer-Emmett-Teller (BET) surface area of HEOs decreased dramatically from 223.5 m^2/g to 85.5 m^2/g (Fig. S3 in Supporting information). High BET specific surface area of HEO-Origin provides abundant active sites, facilitating infiltration of electrolyte into catalyst interior and endowing catalyst with excellent catalytic performance [21].

X-ray diffraction (XRD) patterns in Fig. 1d confirmed that HEO-Origin exhibited two characteristic diffraction peaks of spinel oxide ($CoFe_2O_4$, JPCDS No. 22–1086). High-resolution TEM (HRTEM) in Fig. 1c revealed that HEO-Origin without obvious lattice fringes, implying HEO-Origin with low-crystallinity. Simultaneously, selected-area electron diffraction (SAED) pattern in Fig. 1e shows that HEO-Origin is only a weak reflect hole, reflecting catalyst is lack of long-range order in the third dimensionality and atomic lattice is irregular arrangement [22,23]. Annealing HEO-Origin under air atmosphere from 300 °C to 900 °C (Fig. S4 in Supporting information), as-obtained catalysts all possess single phase spinel structure of $CoFe_2O_4$, which is similar to *Fd*-3 m structure of $(Co, Cr, Ni, Mn, Fe)_3O_4$ [24]. Raman spectroscopy results showed that HEOs possess five Raman active bands ($A_{1g} + E_g + 3F_{2g}$), locating at 155, 250, 337, 435 and 610 cm^{-1} (Fig. S5 in Supporting information). HEOs Raman spectrum match well with $ZnFe_2O_4$, implying that spinel HEOs was successfully synthesized. During energy-dispersive X-ray (EDS) test, homogeneous ink was dropped on Cu grid. Fig. S6 (Supporting information) showed that Fe, Co, Ni, Mn, Zn and O were all presence in HEO-Origin. EDS element mappings in Fig. 1f confirms that all elements in HEO-Origin were uniformly distributed without phase separation. Elements uniformly distributed endows HEO-Origin with a great number of possible microstates numbers and high configurational entropy [8]. Molar fraction of metal elements was measured by inductively coupled plasma optical emission spectrometry (ICP-OES), which was listed in Table S1 (Supporting information).

Linear sweep voltammetry (LSV) was performed on glassy carbon electrode to investigate electrochemical OER activities, polarization curves are shown in Fig. 2a. Onset potential of HEO-Origin is 1.456 V_{RHE} (reversible hydrogen electrode) far less than that of HEO-500°C (1.514 V_{RHE}). HEO-Origin needs only 265 mV overpotential to achieve 10 mA/cm^2 lower than that of HEO-500°C-air (335 mV). Specific activity of HEO-Origin (0.0396 mA/cm^2_{BET}) is 10 times higher than that of HEO-500°C-air (0.00395 mA/cm^2_{BET}) at 1.525 V_{RHE} (Fig. S7 in Supporting information). OER activities decreased with the increase of heat treatment temperature in Fig. S8 (Supporting information), due to catalyst after thermal annealing exposes fewer reactive sites and possesses a lower surface defect. To verify the role of oxygen vacancies, HEO-Origin was calcined at 500 °C under N_2 atmosphere (HEO-500°C-N_2), corresponding XRD patterns and LSV polarization curve are presented in Fig. S9 (Supporting information). As expected, the OER performance of HEO-500°C-air is poorer than HEO-500°C-N_2, suggesting that oxygen vacancies play a significant role. Fig. S10 (Supporting information) shows that O 1s spectrum is deconvoluted into four characteristic oxygen peaks, O1 at 530 eV is typical for lattice oxygen, O2 at 530.88 eV is assigned to oxygen in hydroxyl groups on the outside of catalysts, O3 at 531.55 eV is associated with defect sites with

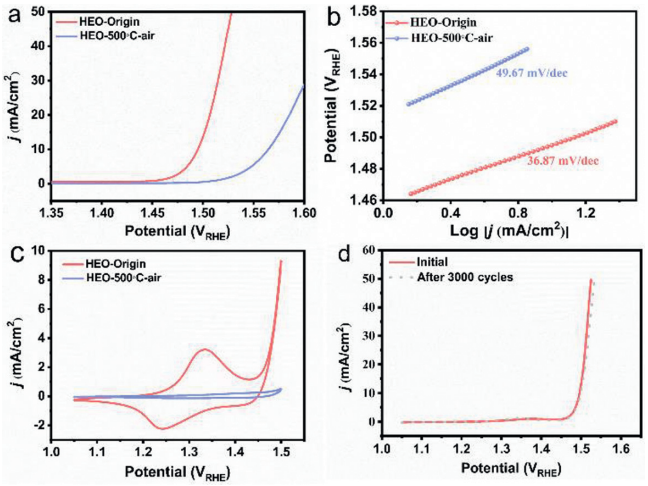

Fig. 2. (a) LSV curves, (b) Tafel slopes and (c) CV curves of HEO-Origin and HEO-500°C-air. (d) LSV curves of HEO-Origin before and after 3000 CVs cycles.

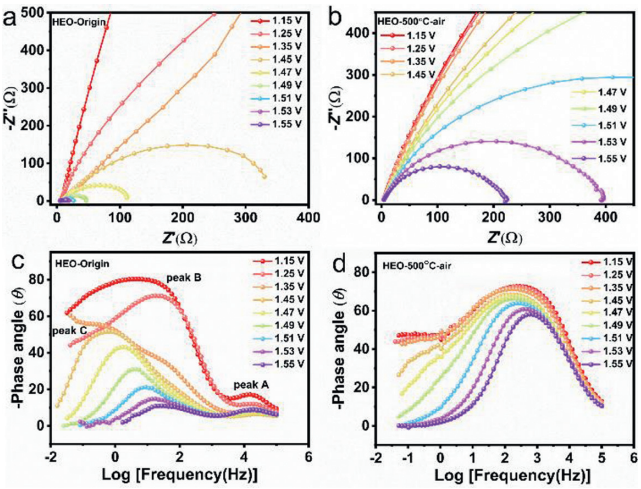

Fig. 3. (a, b) Nyquist plots and (c, d) Bode phase plots of HEO-Origin and HEO-500°C-air at various voltages.

a low oxygen coordinate, O4 at 532.47 eV is attributed to surface-adsorbed oxygen [25–27]. The content of O3 in HEO-Origin (57.1%) is highest in HEO-500°C-N_2 (33.8%) and HEO-500°C-air (21.6%). The excellent catalytic performance of HEO-Origin can be attributed to high specific surface area provides abundant active sites and promotes the infiltration of electrolyte into the interior of catalysts [28], abundant oxygen vacancies tailor electron distribution on the surface of the catalysts and accelate electron transfer [17,29].

Electrochemical surface area (ECSA) was determined by cyclic voltammetry (CV) in Fig. S11 (Supporting Information). C_{dl} of HEO-Origin is 1.79 mF/cm^2 larger than that of HEO-500°C-air (1.28 mF/cm^2). The decrease of ESCA indicates active area of catalyst is dramatically decreased after thermal annealing. After ECSA normalization (Fig. S11d in Supporting Information), OER current of HEO-Origin is still higher than that of HEO-500°C-air, indicating HEO-Origin possesses higher intrinsic activity. Tafel slope of HEO-Origin is 36.87 mV/dec lower than HEO-500°C-air (49.67 mV/dec) in Fig. 2b, implying HEO-Origin with excellent kinetics. In addition, OER is strongly affected by surface properties of catalysts. In Fig. 2c, oxidation peak and reduction peak of HEO-Origin located at 1.334 V and 1.241 V_{RHE}, respectively. Surface reconstruction of HEO-Origin occurs prior to OER. Broad oxidation peak within a potential ranging from 1.2 V_{RHE} to 1.4 V_{RHE}, promoting the oxidation of M^{2+} to M^{3+} or M^{4+}, (Co^{2+}/Co^{3+} peak at 1.1–1.3 V_{RHE} and Co^{3+}/Co^{4+} peak at 1.24–1.54 V_{RHE}) [18,22].

LSV curve of HEO-Origin after 3000 CVs cycles presents negligible degradation in Fig. 2d. Simultaneously, the stability of HEO-Origin loaded on nickel foam was also measured by chronoamperometry in Fig. S12 (Supporting information). After 40,000 s of testing, the current density of HEO-Origin decreased a little from 22.4 mA/cm^2 to 21.53 mA/cm^2. These results indicate that HEO-Origin is promising as a stable and efficient catalyst for electrochemical OER, being able to survive harsh conditions. Constructing low-crystallinity HEO-Origin with rich oxygen vacancies and abundant active sites, endowing catalyst with excellent catalytic activity and stability. The electrocatalytic OER performance of HEO-Origin is even better than most of reported catalysts in Table S2 (Supporting information).

Nyquist plots within a potential range from 1.15 V_{RHE} to 1.55 V_{RHE} are shown in Figs. 3a and b. The related equivalent circuit is presented in Fig. S13 (Supporting information). Table S3 and S4 (Supporting information) display the summary of corresponding fitting date. At high frequency region, the first semicircle can be attributed to R_{film} [30]. The second semicircle or straight line in low frequency region is assigned to charge-transfer resistance (R_{ct}) associated with the overall reaction rate of OER. Nyquist plots of HEO-Origin, HEO-500°C-N_2 and HEO-500°C-air at 1.49 V_{RHE} are presented in Fig. S14 (Supporting information), the smallest R_{ct} of HEO-Origin (37.93 Ω) reveals that HEO-Origin has the fastest electron transfer rate than HEO-500°C-N_2 (510.2 Ω) and HEO-500°C-air (2796 Ω) [31–33]. As a result of HEO-Origin with abundant oxygen vacancies, delocalized electrons close to oxygen vacancies can be excited to conduction band, improving conductivity and electrochemical OER activity [22].

Bode phase plot of HEO-Origin presented in Fig. 3c, phase peak A (10^3–10^5 Hz) has low phase angle, indicating fast charge propagation [34]. Phase peak B (10^1–10^3 Hz) is associated with surface species oxidation at tetrahedral (Td) sites. When potential higher than 1.35 V_{RHE}, phase peak B intensity of HEO-Origin is dramatically decreased, implying its surface is almost completely oxidized. Phase peak C (10^{-1}–10^2 Hz) can be observed When potential higher than 1.45 V_{RHE}. Phase peak C implys the occurrence of OER, which is consistent with its onset potential. However, HEO-500°C-air has no phase peak at low-frequency region in Fig. 3d, indicating that its poor OER activity.

X-ray photoelectron spectroscopy (XPS) is a surface sensitive detective tool, which can be used to investigate valence state [35]. XPS spectrum before and after OER are presented in Figs. S15 and S16 (Supporting information). Figs. 4a and b indicate that the content of O3 is dropped from 57.1% (HEO-Origin) to 21.6% (HEO-500°C-air) after thermal annealing. After stability test, the content of O3 is dropped from 57.1% to 33.9%, still higher than that of HEO-500°C-air (21.6%). Co satellite peaks around 786.3 eV and 803.7 eV in Fig. 4c, implying the existence of high-spin Co^{2+} [36]. Co^{2+} (781.4 eV, 797.1 eV) and Co^{3+} (780.15 eV, 795.95 eV) coexist in HEO-500°C-air (Fig. 4d). However, cabalt only exists as Co^{2+} in HEO-Origin. The content of Co^{2+} in HEO-Origin (100%) is highest than HEO-500°C-N_2 (64.85%, Fig. S17 in Supporting information) and HEO-500°C-air (33.82%). After OER stability test, the binding energy of Co 2p shifts to lower energy indicates a portion of Co^{2+} was oxidized to Co^{3+}. The content of Co^{2+} in HEO-Origin, HEO-500°C-N_2 and HEO-500°C-N_2 is decreased from 100% to 28.42%, 64.85% to 27.48%, 33.82% to 0%, respectively (Figs. 4c and d and Fig. S17 in Supporting information). Fe^{2+} (710.1 eV) and Fe^{3+} (711.5 eV) exist in both HEO-Origin and HEO-500°C-air in Figs. 4e and f. After calcination at 500 °C in air atmosphere, the content of Fe^{2+} is almost unchanged from 24.07% to 24.41%. Besides, Ni 2p spectra is fitted in Figs. 4g and h. In HEO-500°C-air, the binding en-

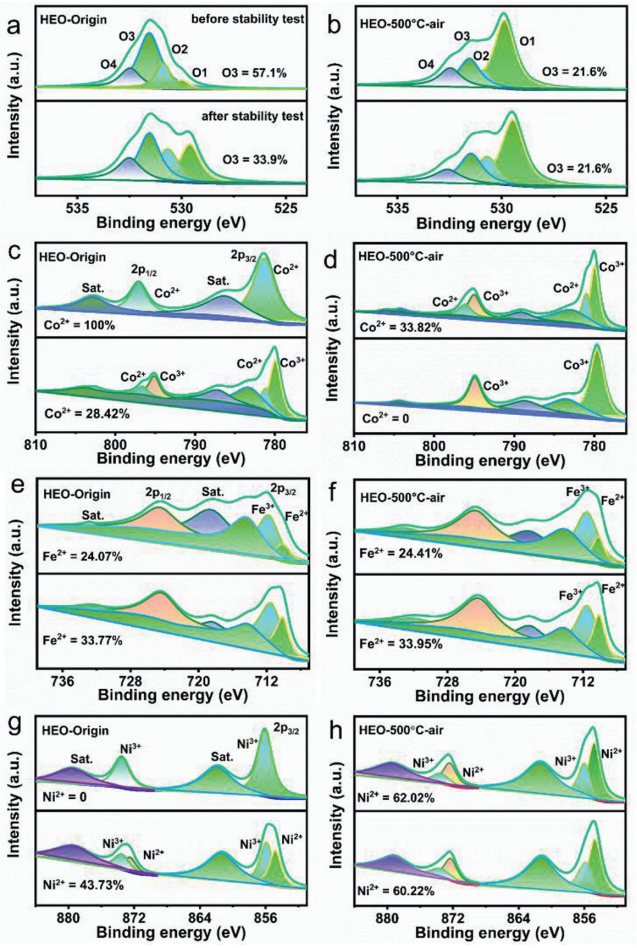

Fig. 4. Fitted (a, b) O 1s spectra, (c, d) Co 2p spectra, (e, f) Fe 2p spectra and (g, h) Ni 2p spectra of HEO-Origin (left) and HEO-500°C-air (right) before (above) and after (bottom) OER stability test.

ergy of 854.8 eV and 872.5 eV are assigned to Ni^{2+}, and the binding energy of 856.0 eV and 873.9 eV are attributed to Ni^{3+}. However, nickel only exists as Ni^{3+} in HEO-Origin, due to Co^{3+} at Td sites of $NiCo_2O_4$ is thermodynamically unstable and prones to convert to Co^{2+}, the existence of Ni^{3+} facilitates the adsorption of OH* intermediate [37]. After stability test, the binding energy of Fe 2p and Ni 2p shift to lower binding energy, implying that a part of Fe^{3+} and Ni^{3+} were reduced to Fe^{2+} and Ni^{2+}, respectively. Surprisingly, HEO-Origin surface was free of zinc cation after OER stability test, due to Zn^{2+} leaches out in KOH electrolyte under high oxidation potential, which is confirmed by Zn XPS spectrum in Fig. S16d (Supporting information). Some cation defect sites may be generated which is also conducive to OER. In comparison, we can detect Zn XPS single, Zn^{2+} in HEO-500°C-air is difficult to completely leaching or dissolving.

The excellent OER performance of HEO-Origin originates from the presence of oxygen vacancies improve the conductivity, enhances OH^- adsorption capacity and serves as efficient active sites [38]. The oxidation of Co^{2+}/Co^{3+} and Co^{3+}/Co^{4+} in HEO-Origin occurs before OER (Fig. 2c) and the content of Co^{3+} is dramatically increased after OER stability test. The increased Co^{3+} indicates theformation of CoOOH, which is highly active for electrochemical OER [38]. Furthermore, Zn^{2+} can be etched at high potential in alkaline electrolyte to create cation vacancies. These synergistic effect together leads to the remarkable OER activity of as-synthesized HEO-Origin.

In this work, we present a facile and effective method to activate surface atoms of HEOs. Constructing low-crystallinity HEO-Origin nanosheet with large specific surface area and rich oxygen vacancies. HEO-Origin requires an overpotential of 265 mV to achieve 10 mA/cm^2 far less than that of HEO-500°C-air, possessing excellent OER activity even better than plenty of reported catalysts. The excellent catalytic performance of HEO-Origin can be attributed to large surface area exposing a great number of active sites, oxygen vacancies efficiently alter catalyst surface electron distribution and accelate electron transfer. The method for activating surface atoms of HEOs provides a new opportunity to discover novel properties of HEOs and promote the application of HEOs in the field of electrocatalysis.

Declaration of competing interest

The authors declare that they have no known competing financial interests or personal relationships that could have appeared to influence the work reported in this paper.

Acknowledgments

This work was supported by the National Natural Science Foundation of China (Nos. U19A2017, 21902047, 51402100, 21825201, 21573066, and 21905088) and the Provincial Natural Science Foundation of Hunan (Nos. 2020JJ5044, 2022JJ10006).

Supplementary materials

Supplementary material associated with this article can be found, in the online version, at doi:10.1016/j.cclet.2022.05.085.

References

[1] C.M. Rost, E. Sachet, T. Borman, et al., Nat. Commun. 6 (2015) 8485.
[2] Y. Zhang, T.T. Zuo, Z. Tang, et al., Prog. Mater. Sci. 61 (2014) 1–93.
[3] C. Oses, C. Toher, S. Curtarolo, Nat. Rev. Mater. 5 (2020) 295–309.
[4] W. Zhang, P.K. Liaw, Y. Zhang, Sci. China Mater. 61 (2018) 2–22.
[5] A. Sarkar, L. Velasco, D. Wang, et al., Nat. Commun. 9 (2018) 3400.
[6] T. Li, Y. Yao, B.H. Ko, et al., Adv. Funct. Mater. 31 (2021) 2010561.
[7] L.H. Liu, N. Li, M. Han, J.R. Han, H.Y. Liang, Rare Metals 41 (2022) 125–131.
[8] A. Sarkar, Q. Wang, A. Schiele, et al., Adv. Mater. 31 (2019) 1806236.
[9] R.Z. Zhang, F. Gucci, H. Zhu, K. Chen, M.J. Reece, Inorg. Chem. 57 (2018) 13027–13033.
[10] H. Chen, J. Fu, P. Zhang, et al., J. Mater. Chem. A 6 (2018) 11129–11133.
[11] D. Bérardan, S. Franger, A.K. Meena, N. Dragoe, J. Mater. Chem. A 4 (2016) 9536–9541.
[12] H. Kwon, M.K. Kabiraz, J. Park, et al., Nano Lett. 18 (2018) 2930–2936.
[13] M. Li, Z. Zhao, T. Cheng, et al., Science 354 (2016) 1414–1419.
[14] J. Fan, Z. Chen, H. Shi, G. Zhao, Chem. Commun. 52 (2016) 4290–4293.
[15] B. Zhang, X. Zheng, O. Voznyy, et al., Science 352 (2016) 333–337.
[16] G. Chen, Y. Zhu, H.M. Chen, et al., Adv. Mater. 31 (2019) 1900883.
[17] Y. Duan, Z.Y. Yu, S.J. Hu, et al., Angew. Chem. Int. Ed. 58 (2019) 15772–15777.
[18] D. Liu, C. Wang, Y. Yu, et al., Chem 5 (2019) 376–389.
[19] Y. Wang, T. Zhou, K. Jiang, et al., Adv. Energy Mater. 4 (2014) 1400696.
[20] L. Li, X. Feng, Y. Nie, et al., ACS Catal. 5 (2015) 4825–4832.
[21] J. Bao, X. Zhang, B. Fan, et al., Angew. Chem. Int. Ed. 54 (2015) 7399–7404.
[22] L. Zhuang, L. Ge, Y. Yang, et al., Adv. Mater. 29 (2017) 1606793.
[23] F. Lei, W. Liu, Y. Sun, et al., Nat. Commun. 7 (2016) 12697.
[24] J. Dąbrowa, M. Stygar, A. Mikuła, et al., Mater. Lett. 216 (2018) 32–36.
[25] S. Zhu, J. Lei, Y. Qin, L. Zhang, L. Lu, RSC Adv. 9 (2019) 13269–13274.
[26] Y. Ding, J. Zhao, W. Zhang, et al., ACS Appl. Energy Mater. 2 (2019) 1026–1032.
[27] P.T. Babar, A.C. Lokhande, M.G. Gang, et al., J. Ind. Eng. Chem. 60 (2018) 493–497.
[28] Y. Sun, S. Gao, F. Lei, et al., Chem. Sci. 5 (2014) 3976–3982.
[29] Y. Wang, Y. Zhang, Z. Liu, et al., Angew. Chem. Int. Ed. 56 (2017) 5867–5871.
[30] S.I. Kim, J.S. Lee, H.J. Ahn, H.K. Song, J.H. Jang, ACS Appl. Mater. Interfaces 5 (2013) 1596–1603.
[31] W.L. Ding, Y.H. Cao, H. Liu, et al., Rare Metals 40 (2021) 1373–1382.
[32] Z.Y. Wang, S.D. Jiang, C.Q. Duan, et al., Rare Metals 39 (2020) 1383–1394.
[33] B. Deng, J. Liang, L. Yue, et al., Chin. Chem. Lett. 33 (2022) 890–892.
[34] P. Jash, A. V, A. Paul, New J. Chem. 43 (2019) 6540–6548.
[35] P. Cai, K. Zou, G. Zou, H. Hou, X. Ji, Nanoscale 12 (2020) 3677–3685.
[36] Z. Li, X. Wu, X. Jiang, et al., Adv. Powder Mater. 1 (2022) 100020.
[37] M. Cui, X. Ding, X. Huang, et al., Chem. Mater. 31 (2019) 7618–7625.
[38] C. Fan, X. Wu, M. Li, et al., Chem. Eng. J. 431 (2022) 133829.